

A New Feature Parametrization for Monocular SLAM using Line Features

Liang Zhao, Shoudong Huang, Lei Yan and Gamini Dissanayake

Abstract

This paper presents a new monocular SLAM algorithm that uses straight lines extracted from images to represent the environment. A line is parametrized by two pairs of azimuth and elevation angles together with the two corresponding camera centres as anchors making the feature initialization relatively straightforward. There is no redundancy in the state vector as this is a minimal representation. A bundle adjustment (BA) algorithm that minimizes the reprojection error of the line features is developed for solving the monocular SLAM problem with only line features. A new map joining algorithm which can automatically optimize the relative scales of the local maps is used to combine the local maps generated using BA. Results from both simulations and experimental datasets are used to demonstrate the accuracy and consistency of the proposed BA and map joining algorithms.

I. INTRODUCTION

Simultaneous localization and mapping (SLAM) is the problem where a mobile robot needs to build a map of its environments and simultaneously use the map to locate itself. Monocular

L. Zhao, S. Huang and G. Dissanayake are with the Centre for Autonomous Systems, Faculty of Engineering and Information Technology, University of Technology, Sydney, NSW 2007, Australia. {Liang.Zhao-1, Shoudong.Huang, Gamini.Dissanayake} @uts.edu.au

L. Yan is with the Institute of Remote Sensing and GIS, School of Earth and Space Science, Peking University, Beijing, China, 100871. lyan@pku.edu.cn

Corresponding author Liang.Zhao-1@uts.edu.au

SLAM is the SLAM problem where the only sensor onboard the robot for observing the environment is a single camera [1], which is more challenging than the SLAM problems using laser sensors and/or RGB-D cameras because of the lack of depth information from the sensor measurements.

Point features are commonly used in monocular SLAM because they are relatively easy to extract, match and represent. However, straight lines are very common in structured environments and arguably provide a better representation of the environment. Line features are less sensitive to motion blur [2], and especially suitable for environments with special structure. Thus, monocular SLAM using straight lines to represent the environment serves as a valuable addition to the suite of SLAM algorithms using monocular cameras.

Feature based SLAM, whether solved using an estimation framework such as the extended Kalman filter (EKF) or an optimization framework, for example bundle adjustment (BA), requires the features to be represented in a state vector using an appropriate parametrization. Most of the line feature parametrizations proposed in the literature, for example traditional Plücker and Plücker based representations, are redundant [3]. Thus it is essential that the relationship between these parameters is imposed as a constraint during the SLAM process. In general, constrained optimization problems are more difficult to be solved than unconstrained optimization problems especially for high dimensional problems. Although constraints can be imposed as a pseudo-measurement in an estimation framework, this can lead to significant numerical issues [4]. Furthermore, some recent research [5] has raised questions about the theoretical validity of the pseudo-measurement approach to imposing constraints in an EKF framework. Clearly, an appropriate minimal representation provides significant advantages in this context. Thus in this paper, we only focus on minimal parametrizations to present line features in 3D environment.

Bartoli and Strum [6] provided an orthonormal representation of the Plücker coordinates using minimal 4 parameters to represent a 3D line feature. A line in the environment is represented as a 3×3 and a 2×2 orthonormal matrices corresponding to its Plücker coordinates, and the 4 parameters can be used to update the Plücker coordinates during BA. Because of using

triangulation for line feature initialization, an accurate initial value of the state vector cannot always be achieved.

In this paper, we propose a new minimal parametrization to describe an environment populated with straight lines, which outperforms the minimal orthonormal representation in [6] in terms of convergence and accuracy. A 3D line can be uniquely defined by the two back-projected planes that correspond to the observed image lines from two camera poses. It is proposed to use two pairs of azimuth and elevation angles that represent the normals of the two back-projected planes, together with the two corresponding camera centres as anchors, to represent a line feature in a 3D environment. The geometric constraint enforcing the fact that three back-projected planes that correspond to the same line feature intersect at the line is used in the observation function to reproject the 3D line feature into the image as captured from an arbitrary viewpoint. Since the azimuth and elevation angles are closely related to the information gathered by processing the image, good initial values of the parameters can always be estimated without any prior although the actual 3D position of the line may not be accurately known.

BA has been the gold standard for monocular SLAM. It is more accurate and consistent as compared to filter based algorithms [7][8]. As camera centres are used as anchors to represent the features in the environment, the proposed line feature parametrization is a minimal feature parametrization for BA where all the camera poses and all the features are used as the parameters of the optimization problem. In this paper, a BA algorithm using the proposed parametrization is developed. The objective function used in the BA algorithm is the total square distances from the set of edge points on the observed image line to the reprojected image line. The least squares problem is shown to have a computational cost independent of the number of edge points that are associated with each of the image lines.

Local map joining has been shown to be one of the efficient strategies for large-scale SLAM [9] where local maps are first built and then combined together to get the global map. In this paper, a map joining algorithm that is able to combine local maps built using BA with the proposed line feature representation to solve large-scale monocular SLAM is also presented. It

is shown that the map joining algorithm can automatically optimize the relative scales of the local maps during the optimization process without introducing any additional variables.

This paper is organized as follows. Section II discusses the recent works related to this paper. Section III states the new parametrization for line features. Section IV details the BA algorithm using the proposed line feature parametrization, while Section V describes the local submap joining algorithm. In Section VI, simulation and experimental results are provided. Finally Section VII concludes the paper.

II. RELATED WORK

There has been significant progress on monocular SLAM using lines as features in the past few years. Some of the work closely related to this paper is discussed below.

Eade and Drummond [10] proposed to describe the edge landmark as edgelet: a very short, locally straight segment of a longer, possibly curved, line. The edgelet is parametrized as a three-dimensional point corresponding to the centre of the edgelet, and a three-dimensional unit vector describing the direction of the edgelet. Each edgelet has 5 DoF which is one degree more than that of an infinite length straight line because the local position of the edgelet on the line is defined. The edgelet parametrization is implemented in a particle-filter SLAM system and it is claimed that this representation is not minimal but the Cartesian representation is found to be more convenient in calculations [10]. Klein and Murray [11] presented a full-3D edge tracking system, also based on the particle filter, while lines are also considered as edgelets in [2] by using the same idea as in [10]. The edge features are added to the map and their resilience to motion blur is exploited to improve tracking under fast motion by using BA [2].

Smith *et al.* [12] described how straight lines can be integrated easily with point features to a monocular extended Kalman filter (EKF) SLAM system. Lines are represented by the locations of the two 3D endpoints. It is clearly not a minimal representation but it does simplify the implementation greatly. It is also more linear than some other representations and hence better for estimation using EKF. A partially-initialized feature is parametrized as the anchor camera

position when the feature was first observed, the two unit vectors giving the directions of the two rays from the projections to the two end points, and the two inverse depths of the two end points. Until a feature is shown to be reliable, it is not converted to a fully initialized feature represented by the two 3D endpoints. Gee and Mayol-Cuevas [13] presents a model-based SLAM system that uses 3D line segments as landmarks. Unscented Kalman filters are used to initialize new line segments and generate a 3D wireframe model of the scene that can be tracked with a robust model-based tracking algorithm. The 3D line segment is initialized by two endpoints with known unit vector directions from the camera centre of projection and unknown depths, which is similar to [12].

In [14], a straight line is represented in terms of a unit vector which indicates the direction of the line, and a vector which designates the point on the line that is closest to the origin, this is similar to the Plücker coordinates. A line segment in the image is represented as two endpoints, and the endpoints of these edges do not necessarily correspond to the endpoints of the three-dimensional line segments. BA using this parametrization was presented.

Lemaire and Lacroix [15] presented a method to incorporate 3D line segments in an EKF SLAM framework for a mobile robot with odometry information. Plücker coordinates are used to represent the 3D lines and new lines are initialized using a delayed Gaussian sum approximation algorithm. Sola *et al.* [16] presents 6-DOF monocular EKF SLAM with undelayed initialization using line landmarks with extensible endpoints, based on the Plücker line parametrization. A careful analysis of the properties of the Plücker coordinates, defined in the projective space, permits their direct usage for undelayed initialization, where immediately after the detection of a line segment in the image, a Plücker line coordinates is incorporated into the map.

A comprehensive comparison of landmark parametrization in the performance of monocular EKF SLAM is presented in [3], where three parametrizations for points and five parametrizations for straight lines are compared, emphasizing on their performance of accuracy and consistency. Only parametrizations that facilitate undelayed feature initialization are compared in the paper. The Plücker coordinates, anchored Plücker coordinates and the parametrizations using two

points such as homogeneous-points lines, anchored homogeneous-points lines and anchored modified-polar-points lines are investigated and it is shown that the anchored modified-polar-points line feature parametrization performs the best in the simulation and experimental results. The anchored Plücker line is also used in combination with the inverse-depth parametrization for point features in the multi robot visual SLAM scenarios [17]. However, all these parametrizations above are not minimal and applying constraints is nontrivial [3].

A more related work is [6], where a minimal line feature parametrization is demonstrated and used in the BA algorithm. The parametrization is based on the orthonormal representation of the Plücker coordinates with two orthonormal matrices and these parameters are updated during BA. Several triangulation methods are proposed in [6] aiming at obtaining a more accurate line feature initial value.

The parametrization proposed in this paper is not based on the Plücker line representation. Instead, the two pairs of azimuth and elevation angles which represent the normals of the two back-projected planes are used as the feature parameters, together with the two corresponding camera centres as anchors. The 3D line can be uniquely defined by the two projective planes which are uniquely defined by the normals and the anchors. Comparing with the existing line feature parametrizations, our parametrization is a minimal representation with 4 parameters in a BA system. The proposed line feature presentation is also close to the measurement space and thus makes the BA algorithm has good convergence properties.

A variety of methods have been proposed in the literature for generating the measurement model and objective function for line feature SLAM. In [2] the two signed orthogonal distances from two points to the reprojected line are used, where the two points are on the image line which are of equal distance from the two sides of the edgelet centre. The distances from the two endpoints are treated as the measurement in [12] and [3]. In [14], the objective function is described as the integration of the distances of all the points between the two endpoints and this integration only depends on the two distances from the endpoints. As described in [18], the observation of a line feature is a set of points in the image, and the total distances from this

set of points to the image line can be replaced by the distances from two weighted points. This idea is also used in [6]. In this paper, the objective function is the original total distances from the observed edge points. However, the least squares optimization is properly formulated such that its computational cost does not depend on how many points are involved in the image line.

III. LINE FEATURE PARAMETRIZATION

In this section we present our line feature parametrization for monocular SLAM. The key idea is to use the normals (azimuth angle and elevation angle) of the two back-projected planes (defined by the image lines and the corresponding camera centres), together with the two anchored camera centres to represent a 3D line feature.

A. Camera Pose Parametrization

A camera pose is represented by rotation angles and translation vector relative to the first camera pose, \mathbf{p}_0 .

The i^{th} camera pose is:

$$\mathbf{p}_i = [\alpha_i \quad \beta_i \quad \gamma_i \quad x_i \quad y_i \quad z_i]^T \quad (1)$$

where $\mathbf{r}_i = [\alpha_i \quad \beta_i \quad \gamma_i]^T$ are the Yaw, Pitch, Roll angles of \mathbf{p}_i and $\mathbf{t}_i = [x_i \quad y_i \quad z_i]^T$ is the translation vector from \mathbf{p}_0 to \mathbf{p}_i (camera centre in \mathbf{p}_0), where $\mathbf{p}_0 = [0 \quad 0 \quad 0 \quad 0 \quad 0 \quad 0]^T$.

B. Line Feature Parametrization

In this paper, we treat a 3D line feature as an infinite line. If the line feature is observed only once, we cannot define a 3D line but can only ascertain that the line is in the back-projected plane with 2 DoF. When the line is observed twice, the total 4 DoF of a 3D line can be defined.

Suppose the line feature \mathbf{L}_j is only observed at \mathbf{p}_{a_1} , we present the line by the back-projected plane and define \mathbf{t}_{a_1} as the anchor of \mathbf{L}_j . The feature is parametrized by:

$$\mathbf{L}_j = [\psi_j^{a_1} \quad \theta_j^{a_1}]^T \quad (2)$$

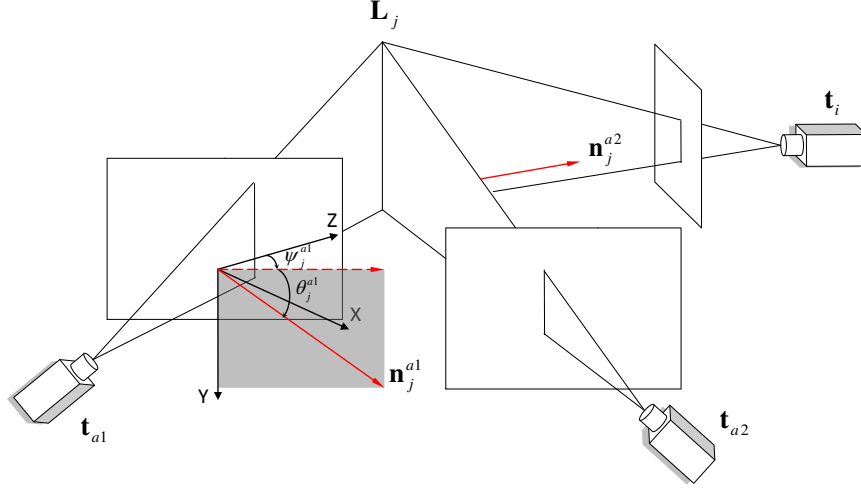


Fig. 1. Line feature parametrization

where ψ_j^{a1} and θ_j^{a1} are the azimuth and elevation angles. So the unit normal vector \mathbf{n}_j^{a1} of the back-projected plane configured by the line \mathbf{L}_j and the anchor \mathbf{t}_{a1} (see Fig. 1) can be computed by using the two angles as

$$\mathbf{n}_j^{a1} = \mathbf{n}(\psi_j^{a1}, \theta_j^{a1}) = \begin{bmatrix} \sin \psi_j^{a1} \cos \theta_j^{a1} \\ \sin \theta_j^{a1} \\ \cos \psi_j^{a1} \cos \theta_j^{a1} \end{bmatrix} \quad (3)$$

and the back-projected plane can be obtained by constraining that the plane contains \mathbf{t}_{a1} .

When the line feature \mathbf{L}_j is observed two times or more, we define the feature as a 3D line with 2 anchors. Suppose the two anchors of \mathbf{L}_j are \mathbf{t}_{a1} and \mathbf{t}_{a2} respectively, then it is described using the two pairs of azimuth and elevation angles which representing the normals of the two planes back-projected from the observed image lines at \mathbf{t}_{a1} and \mathbf{t}_{a2} as follows:

$$\mathbf{L}_j = [\psi_j^{a1} \quad \theta_j^{a1} \quad \psi_j^{a2} \quad \theta_j^{a2}]^T \quad (4)$$

where ψ_j^{a2} and θ_j^{a2} are the azimuth and elevation angles. So the normal direction \mathbf{n}_j^{a2} of the back-projected plane at the anchor \mathbf{t}_{a2} (Fig. 1) can be computed by (3).

C. Anchors Selection for the Line Parametrization

After two observations, the line feature will be fully initialized. Note that in this paper, “fully initialized” simply means it is observed at least twice. It does not mean an accurate 3D location can be estimated from these two measurements. So even when the parallax for a particular line (the angle between the planes) is not large enough to calculate the 3D location, the initialization of the line features in the state vector is still accurate due to the new parametrization we used.

If a line feature is observed more than twice, two of the camera centres are needed to be chosen as the anchors. A simple strategy for anchor selection is to define the two anchors as the camera centres from which \mathbf{L}_j is observed for the first and second time. When we reproject the 3D line feature into the image from any other viewpoint, we use the same geometry constraint as trifocal tensor [18]. The main idea is that all three back-projected planes intersect at the 3D line feature, making it possible to use the two anchored back-projected planes to represent the third one. So at most two of the three planes are linearly independent.

When the motion of the camera does not gain enough parallax for a particular line, which means all the three back-projected planes are nearly the same, any two camera centres can be selected as anchors. In this case, when projecting the line feature from the camera pose which is not one of the anchors, the projective function is still correct since it uses the linear combination of the same two planes to represent the same third plane. However, if the two back-projected planes at the two anchors are the same, but the third one is different, there will be an issue because it is impossible to use linear combination of the same two planes to represent a different plane. In practice, this can cause problem when the two back-projected planes at the two anchors are close to be the same. Therefore anchors need to be selected to avoid this situation.

In this paper, the strategy proposed for selecting the anchors is the following. We first define the anchors as the camera centres where \mathbf{L}_j is observed for the first and second time. When the feature is observed more than two times, we will compare the dot product of every two unit normals of the back-projected planes which represent the cosine of the angle between every two

planes. We will choose the anchors such that the angle between the two anchored back-projected planes is the closest to $\pi/2$ to avoid the above possible problem.

IV. BUNDLE ADJUSTMENT

While the proposed line feature parametrization can be used with an EKF based approach to SLAM, the computational cost will be increased due to the presence of the previous camera centres served as anchors within the state vector. On the other hand, no additional computational cost is introduced in the optimization based approach such as BA where all the camera poses are used as parameters. In this section, the observation function for BA using the new line feature parametrization is first presented. Then the least squares optimization formulation for BA and the initialization of features are briefly outlined.

A. Observation Function for BA

Suppose the line feature \mathbf{L}_j is parametrized by $[\psi_j^{a_1} \ \theta_j^{a_1} \ \psi_j^{a_2} \ \theta_j^{a_2}]^T$ with the two anchors \mathbf{t}_{a_1} and \mathbf{t}_{a_2} , respectively. The normalized image line \mathbf{l}_j^i projected from \mathbf{L}_j at \mathbf{p}_i can be represented as:

$$\mathbf{l}_j^i = \frac{\mathbf{l}_j^i}{\sqrt{(a_j^i)^2 + (b_j^i)^2}} \quad (5)$$

$$\mathbf{l}_j^i = [a_j^i \ b_j^i \ c_j^i]^T = K^{-T} R_i \mathbf{n}_j^i \quad (6)$$

where \mathbf{n}_j^i is the normal of the back-projected plane of feature \mathbf{L}_j at \mathbf{p}_i which can be computed as

$$\mathbf{n}_j^i = \begin{cases} \mathbf{n}_j^{a_1} = \mathbf{n}(\psi_j^{a_1}, \theta_j^{a_1}), & \text{if } i = a_1 \\ \mathbf{n}_j^{a_2} = \mathbf{n}(\psi_j^{a_2}, \theta_j^{a_2}), & \text{if } i = a_2 \\ (\mathbf{t}_{a_2} - \mathbf{t}_i)^T \mathbf{n}_j^{a_2} \mathbf{n}_j^{a_1} - (\mathbf{t}_{a_1} - \mathbf{t}_i)^T \mathbf{n}_j^{a_1} \mathbf{n}_j^{a_2}, & \text{else} \end{cases} \quad (7)$$

where $\mathbf{n}_j^{a_1}$ and $\mathbf{n}_j^{a_2}$ are the unit vectors which represents the normals of the back-projected plane of \mathbf{L}_j at the two anchors \mathbf{t}_{a_1} and \mathbf{t}_{a_2} computed using (3). R_i and \mathbf{t}_i are the rotation matrix and the translation vector of \mathbf{p}_i , respectively. K is the camera calibration matrix.

The first two equations in (7) are obvious. For the last equation of (7), an idea similar to trifocal tensor [18] is used to compute the back-projected plane from the existing two back-projected planes, and then project the plane to get the image line. The details are as follows.

First we transfer the origin of the world coordinates to \mathbf{t}_i . Suppose π_j^i , $\pi_j^{a_1}$ and $\pi_j^{a_2}$ are the three back-projected planes of \mathbf{L}_j at \mathbf{t}_i , \mathbf{t}_{a_1} and \mathbf{t}_{a_2} , respectively. Since the image lines in the three images are derived from the same line \mathbf{L}_j , it follows that these three back-projected planes are not independent but must intersect at this line in 3-space. This intersection constraint can be expressed algebraically by the requirement that the 4×3 matrix $M = [\pi_j^i \quad \pi_j^{a_1} \quad \pi_j^{a_2}]$ has at most rank 2. The matrix M can be expressed by

$$M = \begin{bmatrix} \mathbf{n}_j^i & \mathbf{n}_j^{a_1} & \mathbf{n}_j^{a_2} \\ 0 & -(\mathbf{t}_{a_1} - \mathbf{t}_i)^T \mathbf{n}_j^{a_1} & -(\mathbf{t}_{a_2} - \mathbf{t}_i)^T \mathbf{n}_j^{a_2} \end{bmatrix} \quad (8)$$

where \mathbf{n}_j^i is the normal of the back-projected plane at \mathbf{t}_i .

Now we can use $\pi_j^{a_1}$ and $\pi_j^{a_2}$ to represent π_j^i . And the normal \mathbf{n}_j^i can be computed as

$$\mathbf{n}_j^i = (\mathbf{t}_{a_2} - \mathbf{t}_i)^T \mathbf{n}_j^{a_2} \mathbf{n}_j^{a_1} - (\mathbf{t}_{a_1} - \mathbf{t}_i)^T \mathbf{n}_j^{a_1} \mathbf{n}_j^{a_2}. \quad (9)$$

This is the last equation of (7).

The above observation function is equivalent to the observation function for Plücker coordinates. Suppose the Plücker matrix L_j computed from the intersection of plane $\pi_j^{a_1}$ and $\pi_j^{a_2}$ is

$$L_j = \pi_j^{a_2} (\pi_j^{a_1})^T - \pi_j^{a_1} (\pi_j^{a_2})^T. \quad (10)$$

So

$$[l_{14} \ l_{42} \ l_{34}]^T = (\mathbf{t}_{a_2} - \mathbf{t}_i)^T \mathbf{n}_j^{a_2} \mathbf{n}_j^{a_1} - (\mathbf{t}_{a_1} - \mathbf{t}_i)^T \mathbf{n}_j^{a_1} \mathbf{n}_j^{a_2} \quad (11)$$

where $l_{i,j}$ is the i^{th} row and j^{th} column element of Plücker matrix L_j .

As described in [18], $[l_{14} \ l_{42} \ l_{34}]^T = [l_{23}^* \ l_{13}^* \ l_{12}^*]^T$, where $[l_{23}^* \ l_{13}^* \ l_{12}^*]^T$ are the elements from the dual Plücker matrix L_j^* computed by joining two points. $[l_{23}^* \ l_{13}^* \ l_{12}^*]^T$ is also the normal vector \mathbf{n}_j^i of the plane back projected from \mathbf{t}_i [3]. This is equivalent to (9).

Using the observation function for Plücker coordinates in [3], the image line projected at \mathbf{t}_i can be computed as

$$\mathbf{l}_j^i = K^{-T} R_i ([l_{14} \ l_{42} \ l_{34}]^T - \mathbf{0} \times [l_{23} \ l_{13} \ l_{12}]^T) = K^{-T} R_i \mathbf{n}_j^i. \quad (12)$$

This is equivalent to (6).

B. Objective Function and Least Squares Optimization

In the image, each image line consists of a set of edge points. So the objective function should be the total square distances of these edge points to the reprojected image line computed from the observation function, and should be minimized during the least squares optimization.

Suppose the observed image line projected from \mathbf{L}_j at \mathbf{p}_i consists of a set of edge points $\{\mathbf{x}_k\}, k = 1 \cdots n$ where

$$\mathbf{x}_k = [u_k \ v_k \ 1]^T \quad (13)$$

with (u_k, v_k) be the image coordinate of the edge point.

The least squares optimization problem in BA is to minimize:

$$\|\xi\|_{\Sigma_{ij}^{-1}}^2 = \sum_{ij} (\varepsilon_j^i)^T \Sigma_{ij}^{-1} (\varepsilon_j^i) \quad (14)$$

where ε_j^i is the signed distance vector from the set of edge points $\{\mathbf{x}_k\}$ to each reprojected image line $f(\mathbf{P})$ and Σ_{ij} is the associated covariance matrix. ε_j^i can be computed by

$$\varepsilon_j^i = [\epsilon_1 \cdots \epsilon_k \cdots \epsilon_n]^T = X^T f(\mathbf{P}) \quad (15)$$

where

$$\epsilon_k = \mathbf{x}_k^T f(\mathbf{P}) \quad (16)$$

and

$$X = [\mathbf{x}_1 \cdots \mathbf{x}_k \cdots \mathbf{x}_n]. \quad (17)$$

Here f is the observation function, \mathbf{P} is the state vector and $\mathbf{l}_j^i = f(\mathbf{P})$ is the reprojected image line computed by using (5), (6) and (7).

1) *Weight*: In the least squares formulation (14), each signed distance vector is treated as an observation. Now we use the uncertainty of the edge points to compute the uncertainty of this observation.

Suppose the noises of u_k and v_k are n_u, n_v which are zero-mean Gaussian

$$n_u \sim N(0, \delta^2), \quad n_v \sim N(0, \delta^2). \quad (18)$$

Then the covariance matrix of \mathbf{x}_k is

$$C_{\mathbf{x}_k} = \text{diag}(\delta^2, \delta^2, 0). \quad (19)$$

By (16) the variance of ϵ_k is

$$\omega_k = f(\mathbf{P})^T C_{\mathbf{x}_k} f(\mathbf{P}). \quad (20)$$

Because the reprojected image line $f(\mathbf{P})$ has already been normalized in (5), we have

$$\omega_k = \delta^2. \quad (21)$$

So the weight Σ_{ij}^{-1} in (14) is

$$\Sigma_{ij}^{-1} = [\text{diag}(\omega_1, \dots, \omega_k, \dots, \omega_n)]^{-1} = \frac{1}{\delta^2} I. \quad (22)$$

2) *Linearization*: For simplification, we omit the i and j which represent the pose ID and feature ID respectively and only consider one term in (14). Suppose m is the iteration number and \mathbf{P}_m is the state vector estimated at the m^{th} iteration, we assume that the observation function f is linearized at \mathbf{P}_m by

$$f(\mathbf{P}_m + \Delta_m^{m+1}) \approx f(\mathbf{P}_m) + J_{\mathbf{P}_m} \Delta_m^{m+1} \quad (23)$$

where $J_{\mathbf{P}_m}$ is the linear mapping represented by the Jacobian matrix $\partial f / \partial \mathbf{P}$ evaluate at \mathbf{P}_m .

Substitute (23) into (15), we get

$$X^T f(\mathbf{P}_m + \Delta_m^{m+1}) \approx \varepsilon_m + X^T J_{\mathbf{P}_m} \Delta_m^{m+1} \quad (24)$$

where $\varepsilon_m = X^T f(\mathbf{P}_m)$. Then the problem changes to minimize $\|\varepsilon_m + X^T J_{\mathbf{P}_m} \Delta_m^{m+1}\|_{\Sigma^{-1}}^2$, which is a linear least squares problem. So the update Δ_m^{m+1} from the m^{th} iteration to the $(m+1)^{th}$ iteration can be computed as

$$(X^T J_{\mathbf{P}_m})^T \Sigma^{-1} (X^T J_{\mathbf{P}_m}) \Delta_m^{m+1} = -(X^T J_{\mathbf{P}_m})^T \Sigma^{-1} \varepsilon_m. \quad (25)$$

From (15), (22) and (25), we can get

$$J_{\mathbf{P}_m}^T E J_{\mathbf{P}_m} \Delta_m^{m+1} = -J_{\mathbf{P}_m}^T E f(\mathbf{P}_m) \quad (26)$$

where E is a 3×3 symmetric matrix which can be computed by

$$E = X X^T = \sum_{k=1}^n \mathbf{x}_k \mathbf{x}_k^T. \quad (27)$$

The information matrix of \mathbf{P}_m can be computed by

$$I_{\mathbf{P}_m} = \frac{1}{\delta^2} J_{\mathbf{P}_m}^T E J_{\mathbf{P}_m}. \quad (28)$$

So we can see from (26) that no matter how many edge points specify the observed image line, the computational cost will be almost the same during the least squares optimization because E is a 3×3 matrix which can be easily computed by (27).

C. Image Line Fitting

The observed image line \mathcal{L}_j^i consisting of the set of edge points $\{\mathbf{x}_k\}$ can be fitted as the right null-vector of the matrix A

$$A \mathcal{L}_j^i = \mathbf{0} \quad (29)$$

where $A = E - \zeta_0 W$, $W = \text{diag}(1, 1, 0)$, and ζ_0 is the minimum root of the equation $\det(E - \zeta W) = 0$ ([18]) computed as the smaller one of the non-infinity generalized eigenvalues of E .

D. Line Feature Initialization

If the line feature \mathbf{L}_j is observed only once at \mathbf{p}_{a_1} , then \mathbf{t}_{a_1} is its anchor and \mathbf{L}_j can be initialized as

$$\begin{cases} \psi_j^{a_1} = \text{atan2}(x_j^{a_1}, z_j^{a_1}) \\ \theta_j^{a_1} = \text{atan2}(y_j^{a_1}, \sqrt{(x_j^{a_1})^2 + (z_j^{a_1})^2}) \end{cases} \quad (30)$$

$$\mathbf{n}_j^{a_1} = [x_j^{a_1} \quad y_j^{a_1} \quad z_j^{a_1}]^T = (K R_{a_1})^T \mathbf{l}_j^{a_1} \quad (31)$$

where $\mathbf{l}_j^{a_1}$ is the image line of \mathbf{L}_j observed at \mathbf{p}_{a_1} fitted by using (29).

If \mathbf{L}_j is observed at least twice with anchors \mathbf{t}_{a_1} and \mathbf{t}_{a_2} , then the other two parameters $[\psi_j^{a_2} \quad \theta_j^{a_2}]^T$ can be initialized the same way as using (30) and (31).

It is clear that when using the proposed feature parametrization, the initial values of the line feature parameters are always accurate even if the parallax is small.

V. LOCAL SUBMAP JOINING ALGORITHM

BA is computationally intractable for very large-scale problems no matter which feature parametrization is used. Local map joining has shown to be an efficient strategy for large-scale SLAM. Most of the existing map joining algorithms such as [9][19][20] are for joining point features local maps and require the scale to be consistent among the local maps. In [21], a map joining algorithm that can automatically determine the relative scale during the optimization process is proposed. This section extends the map joining algorithm in [21] for joining the line feature local maps.

A. Local Map Building

First step is to divide original data into groups to build local maps using BA with the new line feature parametrization. The first pose in each of such groups is chosen as the origin of the corresponding local map, $[0 \ 0 \ 0 \ 0 \ 0 \ 0]^T$. The last pose of the l^{th} local map is selected as the first pose of the $(l+1)^{th}$ local map such that the local maps can be linked together.

When performing BA, at least 7 DoF, namely rotation, translation and scale should be fixed [22]. The first pose defines the rotation and translation, while one more parameter is needed to fix the scale. We choose the z value of the translation from the first pose to the second pose z_{l2}^L for this purpose. Typically this is the largest element in the translation vector $\mathbf{t}_{l2}^L = [x_{l2}^L \ y_{l2}^L \ z_{l2}^L]^T$. Setting $z_{l2}^L = 1$ defines the scale of the local map.

B. Deleting Features and Poses from Local Maps

It is unnecessary to include all the poses and features of the local maps in the state vector for map joining because only part of the poses and features in local maps contain useful information relating to the global map:

- “Common features” that appear in at least two local maps;
- The end pose of each local map;
- Translation of the second pose and all the anchors of the “common features”;
- Information matrix corresponding to all the above variables (computed using Schur complement).

Here, the translation of the second pose is kept because it contains the scale of the local map built by BA, and this scale needs to be present and used in the map joining process (see details in Section V-C). Usually, the translation of the second pose is also an anchor for some features.

The map joining algorithm we proposed here follows the idea of [9], that is, using each local map together with its information matrix as an integrated observation to update all the poses and features involved in the global map. This is different from the hierarchical SLAM [23] where each local map is treated as a fixed configuration and the global optimization only optimize the coordinate frames of the local maps. Thus the common features appear in at least two local maps contain important information for optimizing the global map. Removing the unnecessary features and poses from the local maps as above will reduce the computational effort required in map joining but will not affect the optimality of the global map. However if some of the common

features are also removed, then the map joining result will no longer be optimal although the computational cost of map joining can be reduced further.

After removing the unnecessary elements, the l^{th} local map can be represented as

$$[\mathbf{X}_l^L \quad I_l^L] \quad (32)$$

where \mathbf{X}_l^L is the vector of all the kept poses and features, I_l^L is the information matrix for \mathbf{X}_l^L .

For the l^{th} local map, \mathbf{X}_l^L contains:

- The end pose $\mathbf{p}_{le}^L = [\alpha_{le}^L \quad \beta_{le}^L \quad \gamma_{le}^L \quad x_{le}^L \quad y_{le}^L \quad z_{le}^L]^T$;
- Common features \mathbf{L}_{lj}^L observed in at least two local maps, include features $[{}^L\psi_{lj}^{a_1} \quad {}^L\theta_{lj}^{a_1}]^T$ observed only once and fully initialized 3D line features $[{}^L\psi_{lj}^{a_1} \quad {}^L\theta_{lj}^{a_1} \quad {}^L\psi_{lj}^{a_2} \quad {}^L\theta_{lj}^{a_2}]^T$ in the l^{th} local map;
- Translation of the second pose and all the anchors of the kept line features. The i^{th} translation of the pose is denoted as $\mathbf{t}_{li}^L = [x_{li}^L \quad y_{li}^L \quad z_{li}^L]^T$.

Here a local map may contain line features which are not fully initialized. However, in map joining, only the common features that appear in at least two local maps are used (since the features only appear in one local map does not contribute to the map joining result). So if a feature is not fully initialized in one local map, it will be fully initialized in the map joining since it will definitely appear in another local map.

C. Observation Function for Local Submap Joining

The n local maps $[\mathbf{X}_l^L \quad I_l^L]$, $l = 1, \dots, n$ are treated as n observations in the map joining process ([9]). The observation function for the map joining is given by

$$\mathbf{X}^L = H(\mathbf{X}^G) + \mathbf{w} \quad (33)$$

where

$$\mathbf{X}^L = [\mathbf{X}_1^L \quad \dots \quad \mathbf{X}_n^L]^T \quad (34)$$

contains all the local maps as the observation. \mathbf{w} is the noise of the observation and its covariance matrix Σ is given by

$$\Sigma^{-1} = I^L = \text{diag}(I_1^L, \dots, I_n^L). \quad (35)$$

We use \mathbf{X}^G to denote the parameters in the global map. It contains the poses and line features in the global coordinate frame which is the coordinate frame of the first local map. Comparing with the observation \mathbf{X}^L , \mathbf{X}^G contains:

$$\begin{aligned} \bullet \quad \mathbf{p}_{le}^L &\rightarrow \mathbf{p}_{le}^G = [\alpha_{le}^G \quad \beta_{le}^G \quad \gamma_{le}^G \quad x_{le}^G \quad y_{le}^G \quad z_{le}^G]^T \\ \bullet \quad \{\mathbf{L}_{lj}^L\} &\rightarrow \mathbf{L}_j^G = [{}^G\psi_j^{A_1} \quad {}^G\theta_j^{A_1} \quad {}^G\psi_j^{A_2} \quad {}^G\theta_j^{A_2}]^T \\ \bullet \quad \mathbf{t}_{li}^L &\rightarrow \mathbf{t}_{li}^G = [x_{li}^G \quad y_{li}^G \quad z_{li}^G]^T. \end{aligned} \quad (36)$$

There are two main differences between \mathbf{X}^L and \mathbf{X}^G :

(1) All the variables in the state vector \mathbf{X}^G are in the global coordinate frame which is the coordinate frame of the first local map;

(2) $\{\mathbf{L}_{lj}^L\} \rightarrow \mathbf{L}_j^G$ means all the features \mathbf{L}_{lj}^L in different local maps representing the same feature \mathbf{L}_j will be one feature \mathbf{L}_j^G in the global state vector. The anchor selection strategy described in Section III-C is also used to avoid singularity in the observation function, so the anchors of line features in the global map (with ID A_1 and A_2) may be different from the anchors in the local maps. Note that part of features $[{}^L\psi_{lj}^{a_1} \quad {}^L\theta_{lj}^{a_1}]^T$ which have been observed only once in one local map, will be fully initialized 3D line features $[{}^G\psi_j^{A_1} \quad {}^G\theta_j^{A_1} \quad {}^G\psi_j^{A_2} \quad {}^G\theta_j^{A_2}]^T$ in \mathbf{X}^G since they are also observed in other local maps and thus have two anchors.

Here we use superscript G for the variables in the global coordinates and superscript L for the variables in local map coordinates. Suppose l represents the local map ID, i represents the pose translation ID, e represents the end pose of local map and j represents the feature ID. Let A (A_1 or A_2) represents the global ID of the anchor of the line feature in the global map, while a (a_1 or a_2) represents the local ID of the anchor of the feature in the local map. Then the observation function $\mathbf{X}^L = H(\mathbf{X}^G)$ can be written as follows:

The end pose of the $(l-1)^{th}$ local map is the 1^{st} pose of the l^{th} local map. So the rotation of the end pose of the l^{th} local map, in the l^{th} local map coordinates can be computed as

$$\mathbf{r}(\alpha_{le}^L, \beta_{le}^L, \gamma_{le}^L) = R_{le}^G (R_{(l-1)e}^G)^T \quad (37)$$

where $R_{(l-1)e}^G$ and R_{le}^G are the rotation matrices of the end pose of the $(l-1)^{th}$ and l^{th} local map in global coordinates, respectively.

The translations of the 2^{nd} , end pose and anchors of the l^{th} local map, in the l^{th} local map coordinates can be computed as

$$\mathbf{t}_{li}^L = R_{(l-1)e}^G (\mathbf{t}_{li}^G - \mathbf{t}_{(l-1)e}^G) / \hat{z}_{l2}^L \quad (38)$$

where \mathbf{t}_{li}^G is the i^{th} translation of the l^{th} local map, and $\mathbf{t}_{(l-1)e}^G$ is the translation of the end pose of the $(l-1)^{th}$ local map, all in global coordinates.

Here \hat{z}_{l2}^L in (38) is the relative scale between the local map and global map which is given in

$$[\hat{x}_{l2}^L \ \hat{y}_{l2}^L \ \hat{z}_{l2}^L]^T = R_{(l-1)e}^G (\mathbf{t}_{l2}^G - \mathbf{t}_{(l-1)e}^G) \quad (39)$$

where \mathbf{t}_{l2}^G is the 2^{nd} translation of the l^{th} local map in global coordinates.

For the scale factor \hat{z}_{l2}^L , when computing the i^{th} translation in the l^{th} local map in the l^{th} local map coordinates as $\hat{\mathbf{t}}_{li}^L = R_{(l-1)e}^G (\mathbf{t}_{li}^G - \mathbf{t}_{(l-1)e}^G)$ by using the variables in the global state vector, $\hat{\mathbf{t}}_{li}^L$ is with the scale of the global map, however \mathbf{t}_{li}^L in the observation vector is with the scale of the l^{th} local map. As we fix the z value of the second pose $z_{l2}^L = 1$ when performing local map BA, the l^{th} local map is with the scale $z_{l2}^L = 1$. So we can compute the 2^{nd} translation of the l^{th} local map with the scale of the global map as (39). Thus the scale between global map and the l^{th} local map is $\hat{z}_{l2}^L / z_{l2}^L = \hat{z}_{l2}^L / 1 = \hat{z}_{l2}^L$. Then \mathbf{t}_{li}^L with the scale of the l^{th} local map can be computed as (38). The scale between different local maps will be optimized during the least squares optimization process.

The pair of azimuth and elevation angles $[\psi_{lj}^a \ \theta_{lj}^a]$ of feature \mathbf{L}_{lj}^L in the l^{th} local map, in

the l^{th} local map coordinates can be easily computed from the normal vector as

$$\begin{cases} {}^L\psi_{lj}^a = \text{atan2}({}^Lx_{lj}^a, {}^Lz_{lj}^a) \\ {}^L\theta_{lj}^a = \text{atan2}({}^Ly_{lj}^a, \sqrt{({}^Lx_{lj}^a)^2 + ({}^Lz_{lj}^a)^2}) \end{cases} \quad (40)$$

$$[{}^Lx_{lj}^a \ {}^Ly_{lj}^a \ {}^Lz_{lj}^a]^T = s \ {}^L\mathbf{n}_{lj}^a. \quad (41)$$

Here ${}^L\mathbf{n}_{lj}^a$ is the vector which represents the normal of the back-projected plane of feature \mathbf{L}_{lj}^L at anchor \mathbf{t}_{la}^G in the l^{th} local map, in the l^{th} local map coordinates, given by

$${}^L\mathbf{n}_{lj}^a = \begin{cases} R_{(l-1)e}^G {}^G\mathbf{n}_j^A, & \text{if } a = A \\ R_{(l-1)e}^G {}^G\mathbf{n}_{lj}^a, & \text{if } a \neq A. \end{cases} \quad (42)$$

where ${}^G\mathbf{n}_j^A$ is the unit vector which represents the normal of the back-projected plane of feature \mathbf{L}_j^G at anchor \mathbf{t}_A^G in the global coordinates

$${}^G\mathbf{n}_j^A = \mathbf{n}({}^G\psi_j^A, {}^G\theta_j^A). \quad (43)$$

${}^G\mathbf{n}_{lj}^a$ is the normal of the back-projected plane of feature \mathbf{L}_{lj}^L at anchor \mathbf{t}_{la}^G in the l^{th} local map, in global coordinates and can be computed as

$${}^G\mathbf{n}_{lj}^a = (\mathbf{t}_{A_2}^G - \mathbf{t}_{la}^G)^T {}^G\mathbf{n}_j^{A_2} {}^G\mathbf{n}_j^{A_1} - (\mathbf{t}_{A_1}^G - \mathbf{t}_{la}^G)^T {}^G\mathbf{n}_j^{A_1} {}^G\mathbf{n}_j^{A_2} \quad (44)$$

where ${}^G\mathbf{n}_j^{A_1}$ and ${}^G\mathbf{n}_j^{A_2}$ represent the two normal vectors, $\mathbf{t}_{A_1}^G$ and $\mathbf{t}_{A_2}^G$ represent the two anchors of feature \mathbf{L}_j^G in the global map, in the global coordinates. While \mathbf{t}_{la}^G is the anchor of feature \mathbf{L}_{lj}^L in the l^{th} local map, in the global coordinates.

The details about the derivation of (44) are similar to that of observation function (7) described in Section IV-A and are omitted here.

The s in (41) is a sign defined by

$$s = \begin{cases} +1, & \text{if } {}^L\varphi_{lj}^a \leq \pi/2 \\ -1, & \text{if } {}^L\varphi_{lj}^a > \pi/2 \end{cases} \quad (45)$$

where ${}^L\varphi_{lj}^a$ is the angle between vectors ${}^L\mathbf{n}_{lj}^a$ and ${}^L\bar{\mathbf{n}}_{lj}^a$ computed from the dot product

$${}^L\varphi_{lj}^a = \arccos \left({}^L\bar{\mathbf{n}}_{lj}^a \cdot \frac{{}^L\mathbf{n}_{lj}^a}{\|{}^L\mathbf{n}_{lj}^a\|} \right). \quad (46)$$

Here ${}^L\bar{\mathbf{n}}_{lj}^a$ has the same physical meaning as ${}^L\mathbf{n}_{lj}^a$ but computed by the local map information

$${}^L\bar{\mathbf{n}}_{lj}^a = \mathbf{n}({}^L\psi_{lj}^a, {}^L\theta_{lj}^a) \quad (47)$$

where $[{}^L\psi_{lj}^{a1} \ {}^L\theta_{lj}^{a1}]^T$ is from the measurement vector \mathbf{X}^L .

Here the sign s is used to make the observation function, measurement vector and the information matrix consistent. As we know, both $\pm {}^L\mathbf{n}_{lj}^a$ represents the normal of the same back-projected plane. So for the line feature parametrization proposed in this paper, there are 4 choices of each line feature. This is similar to the orthonormal representation in [6] because $(\pm U, \pm W)$ represent the same Plücker line. In BA, this doesn't matter because BA will converge to one (out of four) correct solution depending on the initial guess. However in the map joining, the normal computed using the observation function must be the same choice as the one in the measurement vector because the local map information matrix obtained through BA is about the particular choice from the BA result. So we first compare the two normal vectors computed from the observation function and the measurement vector, respectively. If the angle between these two normals are more than $\pi/2$, the normal computed from the observation function must be in the opposite direction and thus we define the sign $s = -1$.

D. Least Squares Optimization of Map Joining

Local submap joining for line feature monocular SLAM can now be stated as a least squares problem similar to (14) such that

$$\|\varepsilon\|_{\Sigma^{-1}}^2 = (H(\mathbf{X}^G) - \mathbf{X}^L)^T \Sigma^{-1} (H(\mathbf{X}^G) - \mathbf{X}^L) \quad (48)$$

is minimized.

The measurement vector \mathbf{X}^L consists of all the local maps as shown in (34), the parameter vector \mathbf{X}^G is the global map with all the kept poses and features in the global coordinates as shown in (36), $H(\mathbf{X}^G)$ is the observation function in (33), and Σ^{-1} is given in (35), which is the combination of the information matrices of all the local maps.

E. Initialization for Local Submap Joining Algorithm

To join the l^{th} local map into global map, all the variables in the l^{th} local map need to be initialized in the global coordinates.

For the end pose and translations of anchors,

$$\mathbf{r}(\alpha_{le}^G, \beta_{le}^G, \gamma_{le}^G) = R_{le}^L R_{(l-1)e}^G \quad (49)$$

$$\mathbf{t}_{li}^G = (R_{(l-1)e}^G)^T \mathbf{t}_{li}^L + \mathbf{t}_{(l-1)e}^G. \quad (50)$$

For the pose initialization, we simply assume the relative scale between local map and global map is equal to 1 and let the map joining algorithm adjust the relative scale.

Line features not already present in the global map, can be initialized by

$$\mathbf{n}({}^G\psi_j^A, {}^G\theta_j^A) = (R_{(l-1)e}^G)^T \mathbf{n}({}^L\psi_{lj}^a, {}^L\theta_{lj}^a) \quad (51)$$

with the two anchors $A_1 = a_1$ and $A_2 = a_2$.

If the 3D line feature has already been included in the global map, an anchor changed initialization similar to Section III-C is done to avoid using the linear combination of the same two back-projected planes to represent a different plane in (44). After the anchors are defined, the initialization is the same as using (51).

F. Computational Complexity

As described in [24], suppose there are O_G feature projections as observations from C_G poses. If (26) is solved by Schur complement

$$\begin{bmatrix} U & W \\ W^T & V \end{bmatrix} \begin{bmatrix} \Delta_P \\ \Delta_F \end{bmatrix} = \begin{bmatrix} \mathbf{E}_P \\ \mathbf{E}_F \end{bmatrix} \quad (52)$$

$$(U - WV^{-1}W^T)\Delta_P = \mathbf{E}_P - WV^{-1}\mathbf{E}_F \quad (53)$$

$$V\Delta_F = \mathbf{E}_F - W^T\Delta_P, \quad (54)$$

then the computational complexity of one iteration for the global BA is $\Theta(O_G + O_G C_G + C_G^3)$, where the computational complexity of computing information matrix $J_{\mathbf{P}_m}^T E J_{\mathbf{P}_m}$ is proportional to the number of the observations $\Theta(O_G)$, $\Theta(O_G C_G)$ is the computational complexity of computing the product $WV^{-1}W^T$, and the computational complexity of solving the linear system (53) is $\Theta(C_G^3)$ [8].

For the map joining algorithm, the computational cost consists of two parts: building the local maps and joining the local maps.

Suppose the observations are equally divided to build n local maps. In each local map, there are C_L camera poses and O_L feature projections as observations, with $C_G = n \times C_L$ and $O_G = n \times O_L$. So the computational complexity of building n local maps is $\Theta(O_L + O_L C_L + C_L^3) \times n = \Theta(O_G + \frac{1}{n} O_G C_G + \frac{1}{n^2} C_G^3)$. Obviously the computational complexity of building n local maps is much less than that of a global BA.

For the map joining process, suppose O_M variables are kept from different local maps in (34) as observations, and in the global map there are C_M camera poses or translations. Similar to BA, the computational complexity of computing information matrix is $\Theta(O_M)$. For building the Schur complement, the nonzero elements in each column of matrix W only appear at the two anchors of this corresponding feature in each local map, as well as the first poses of these local maps. So the number of nonzero elements in matrix is also the same as the observations O_M , thus the computational complexity of computing $WV^{-1}W^T$ is $\Theta(O_M C_M)$. In the global map, besides n end poses with full rotation and translation, all the other kept poses are only translations. Thus the computational complexity of solving the linear system depending on the number of poses is $\Theta(\frac{1}{8} C_M^3)$. So for the map joining process, the computational complexity is $\Theta(O_M + O_M C_M + \frac{1}{8} C_M^3)$.

The overall computational complexity of the map joining algorithm is $\Theta(O_G + \frac{1}{n} O_G C_G + \frac{1}{n^2} C_G^3 + O_M + O_M C_M + \frac{1}{8} C_M^3)$.

The complexity gains with respect to global BA obtained from map joining algorithm for Simulation, ETSI Málaga corridor 2.2 Dataset and DLR dataset are shown in Table I.

TABLE I

COMPUTATIONAL COMPLEXITY GAIN OBTAINED FROM MAP JOINING IN COMPARISON WITH GLOBAL BA

Dataset		O_G or O_L	C_G or C_L	n	O_M	C_M	gain
Simulation	Global BA	1763	76				1
	Map joining	440	20	4	328	73	5
Malaga	Global BA	2880	240				1
	Map joining	960	81	3	127	75	19
DLR	Global BA	18950	3298				1
	Map joining	4780	825	4	1093	626	15

For the same dataset, the number and size of local maps also affect the computational complexity of the map joining algorithm. Choosing the suitable number of local maps to minimize the overall computational cost is another interesting research topic [25] and is not discussed here.

VI. SIMULATION AND EXPERIMENTAL RESULTS

Simulation and real datasets have been used to check the validity and accuracy of the BA and map joining algorithms using the proposed line feature parametrization.

A. Simulation Results

The environment is set up as a $11\text{m} \times 11\text{m}$ square corridor with 11m length (10m length inside and 12m length outside), 2m width and 3m high each side (Fig. 2). Besides the $4 \times 4 = 16$ lines located at the intersection of ceiling and wall (or floor and wall) along the corridor, lines of 1m length in every 1m are simulated on the floor and ceiling. And 2m length lines every 1m are simulated on the right and left walls. All the lines on the floor, ceiling and walls are perpendicular to the length direction of the corridor. A $0.3\text{m} \times 0.3\text{m} \times 0.3\text{m}$ box and a $1\text{m} \times$

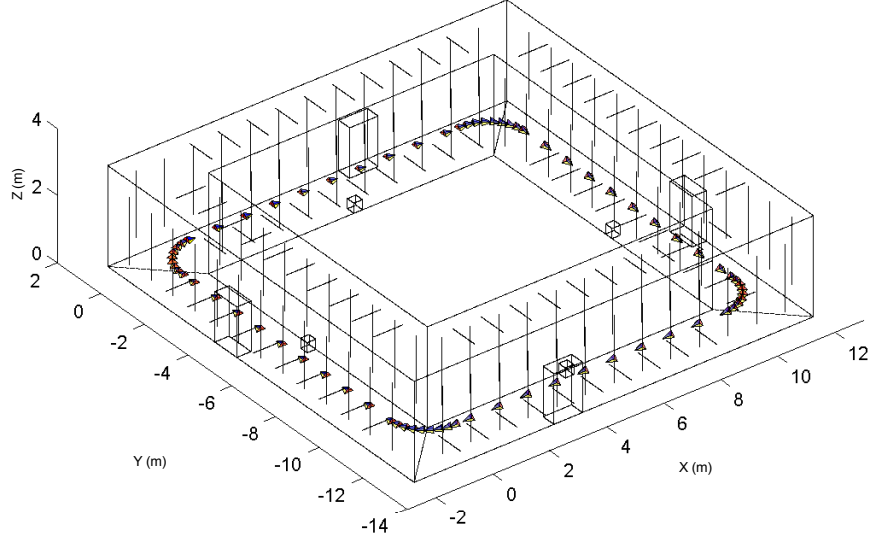


Fig. 2. Simulation environment and robot trajectory

$0.5\text{m} \times 1.5\text{m}$ cabinet are also simulated in each side of the corridor. There are totally 296 lines in the simulation environment.

The robot is simulated as moving in the middle of the corridor with 1m distance each step when moving straight forward, and 0.25m distance and $\pi/16$ rad each step when turning at the corner. There are 76 poses on the square trajectory in total. The camera onboard the robot is assumed to be 0.5m above the ground and look forward. The simulation environment and the trajectory are shown in Fig. 2.

All the lines are projected in the images using the pinhole camera model. The camera is modelled as $[-\pi/4, \pi/4]$ of FOV, $[0, +\infty]$ observation distance, 800×800 image resolution, $[400, 400]$ principle point and $[400, 400]$ focal length, as described in Table II. The lines are sampled as edge points with constant distance 1 pixel along the line direction. A random Gaussian noise with $\sigma = 1$ is added on the theoretical image coordinates of the edge points within the FOV as the observations of the 3D line features. Typical simulated images are shown in Fig. 3.

The simulated image lines in all the 76 simulated images are used in the proposed BA

TABLE II
SENSOR MODEL IN SIMULATION

Parameter	Description
Sensor.FOV = $[-\pi/4, \pi/4]$	FOV: Bearing $[Min, Max]$
Sensor.Distance = $[0, +\infty]$	Observation distance $[Min, Max]$
Sensor.Resolution = $[800, 800]$	Image resolution $[u, v]$
Sensor.PP = $[400, 400]$	Principle point $[P_u, P_v]$ in pixel
Sensor.FL = $[400, 400]$	Focal length $[F_u, F_v]$ in pixel
Sensor.uvNoise = $1 \times randn$	uv Noise Gaussian $\sigma = 1$

algorithm. For the initial value of camera poses, we add $\sigma = 0.05 \text{ rad}$ Gaussian noise on the three rotation angles and multiply a random scale from 0.8 to 1.2 on the relative translation of each step of the ground truth as the initial value. The initial value of the line features is computed by (30) and (31). The result of BA using the proposed line feature parametrization is shown in Fig. 4.

To test the proposed map joining algorithm, the whole dataset is divided into 4 groups to build 4 local maps. Each local map contains about 20 to 21 poses and 67 to 83 line features. BA with proposed line feature parametrization was used to build the 4 local maps. The local submap joining algorithm was then used to build the global map. The map joining result is also shown in Fig. 4. It can be seen that both the map joining result and the BA result are very close to the ground truth.

To check the consistency of the BA and map joining algorithms proposed in this paper, five simulations are run with the same simulation environment and the same noise level for observation and initial value, but each with different random seeds for the noises. All the pose translations of the BA results and the kept translations of the map joining results, together with

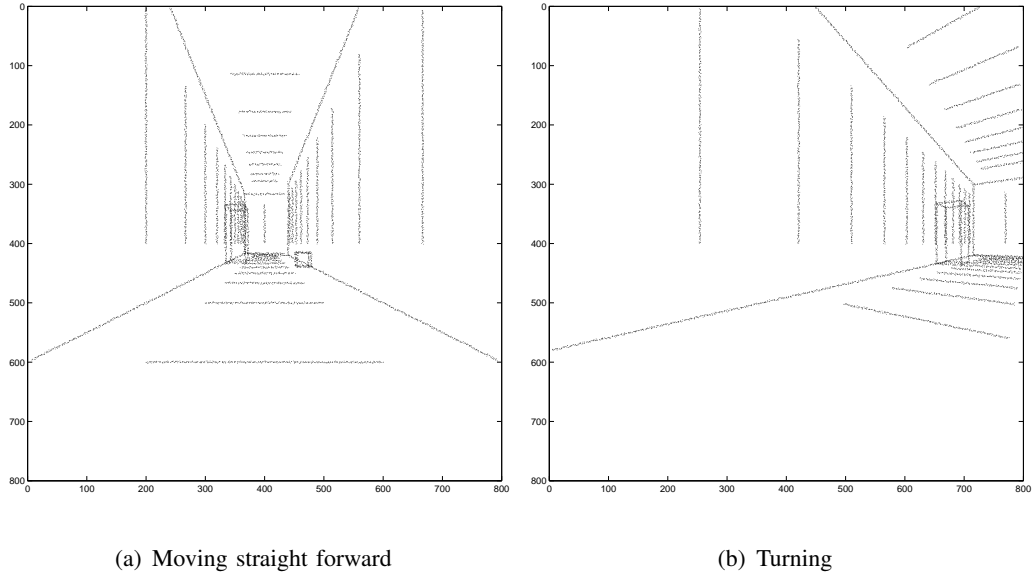


Fig. 3. Simulated images

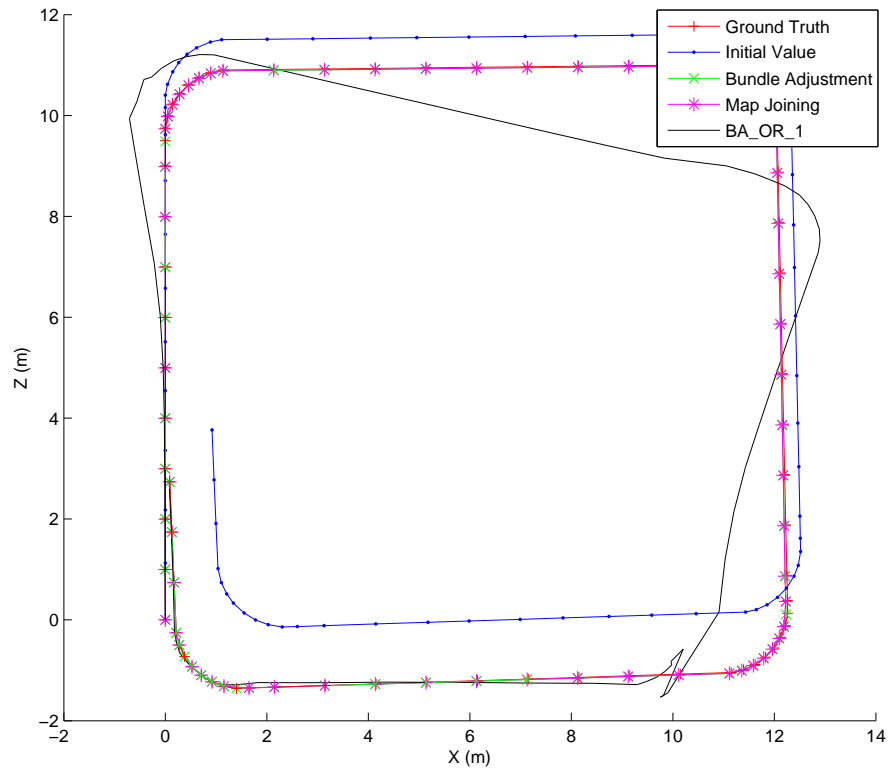


Fig. 4. BA and map joining results of simulation

TABLE III

CONSISTENCY OF BA RESULT BY NEES CHECK (95%)

Run	1	2	3	4	5
Dimensions	224	224	224	224	224
H Bound	267.35	267.35	267.35	267.35	267.35
NEES	205.27	249.17	191.15	210.24	207.72
L Bound	184.44	184.44	184.44	184.44	184.44

TABLE IV

CONSISTENCY OF MAP JOINING RESULT BY NEES CHECK (95%)

Run	1	2	3	4	5
Dimensions	209	209	215	209	215
H Bound	250.93	250.93	257.50	250.93	257.50
NEES	218.03	232.67	224.11	254.92	208.53
L Bound	170.86	170.86	176.28	170.86	176.28

the corresponding information matrix are used to check the consistency [26] of the BA and map joining algorithms using normalised estimation error squared (NEES) [27]. The NEES results are shown in Table III and Table IV together with the associated lower and higher bounds. For the BA results, there are 76 pose translations and state dimension is 224 because the first camera pose and one parameter of the second pose translation are fixed during the least squares optimization. We can see that all the BA results are consistent. For the map joining results, because the anchors of line features may be different, the numbers of the pose translations and the state dimensions are not always the same in different runs.

As comparison, the BA using orthonormal representation (BA_OR) of line features proposed

in [6] is implemented and compared with the BA proposed in this paper using the simulation dataset described above. The camera pose parametrization for the BA_OR is the same as (1) proposed in this paper. And we also use E matrix in (27) instead of the two weighted points [6][18] in the objective function in order to compare with the proposed BA using the same mean square error (MSE) (the objective function defined in (14) divided by the number of line observations).

Table V demonstrates that the BA proposed in this paper (“BA” in Table V) has better convergence properties as compared with BA_OR. In fact, for the BA algorithm proposed in this paper (BA), all the 5 runs converged using only Gauss-Newton (GN) iteration. When using the two poses which are the same as the two anchors in the proposed BA together with the two observations to triangulate each Plücker coordinates as the initial value for BA_OR (“BA_OR_1” in Table V), which means the initial guess and the initial objective function of BA_OR_1 and the proposed BA are the same, all the 5 runs diverged for GN. And when Levenberg-Marquardt (LM) is used, BA_OR_1 take around 2,000 iterations to converge to obvious local minima (see Table V). But when part of the dataset (e.g. 10 images) is used, it can converge for both GN and LM. Then, because the quasi-linear algorithm (QLIN2) proposed in [6] has singularity when all the poses observed that line feature are collinear, the nonlinear triangulation method [6] is used to triangulate the Plücker coordinates as initial value for BA_OR algorithm (“BA_OR_2” in Table V), which is the best initial guess of the line features one can get through initialization without singularity issue. The same as BA_OR_1, neither GN nor LM can converge to the correct results for the whole dataset. At last, we used the line feature parameters of the converged results of the proposed BA to compute the Plücker coordinates as the initial value (“BA_OR_3” in Table V), BA_OR converged for all the 5 runs when only GN is used. This shows that BA_OR needs good initial value of line feature. As an example, the BA_OR_1 result of Run 2 using LM is shown in Fig. 4 as black line.

TABLE V
CONVERGENCE AND MSE OF SIMULATION

	BA	BA_OR.1		BA_OR.2		BA_OR.3
Run	GN	GN	LM	GN	LM	GN
1	199.2081	N	1389.0838	N	1810.6741	199.2081
2	199.6360	N	622.8728	N	1345.6028	199.6360
3	199.5360	N	749.8807	N	2715.6562	199.5360
4	199.8054	N	2364.5208	N	2328.5485	199.8054
5	199.2762	N	888.2551	N	991.8803	199.2762

B. Results using Real Experimental Datasets

For the experimental results, the dataset collected ourselves (FEIT UTS Corridor Dataset) and publicly available datasets (ETSI Málaga corridor 2.2 Dataset [28] and DLR Dataset [29]) are used for the algorithms described in this paper. All the datasets are corridor environment because this kind of environment is mainly described by the line features.

1) *FEIT UTS Corridor Dataset*: For the first experimental result, the dataset is collected in the corridor of level 6, building 2 at University of Technology, Sydney (UTS). The Dragonfly DR2-HIBW/HICOL-XX camera is used to capture the images and the image resolution is 1024×768 . The calibration is done by using the Matlab Automatic Camera Calibration Toolbox [30]. Then the images are undistorted using the calibration parameters. One of the undistorted images is shown in Fig. 5(a).

The Canny edge detection [31] is used to get the edge points in the image. The edge detection result is shown in Fig. 5(b). The image lines are selected by defining the endpoints of each image line manually. And then, the edge points are linked by searching the area defined by the endpoints of each image line and finding the edge points from which the distances are less than 2 pixels

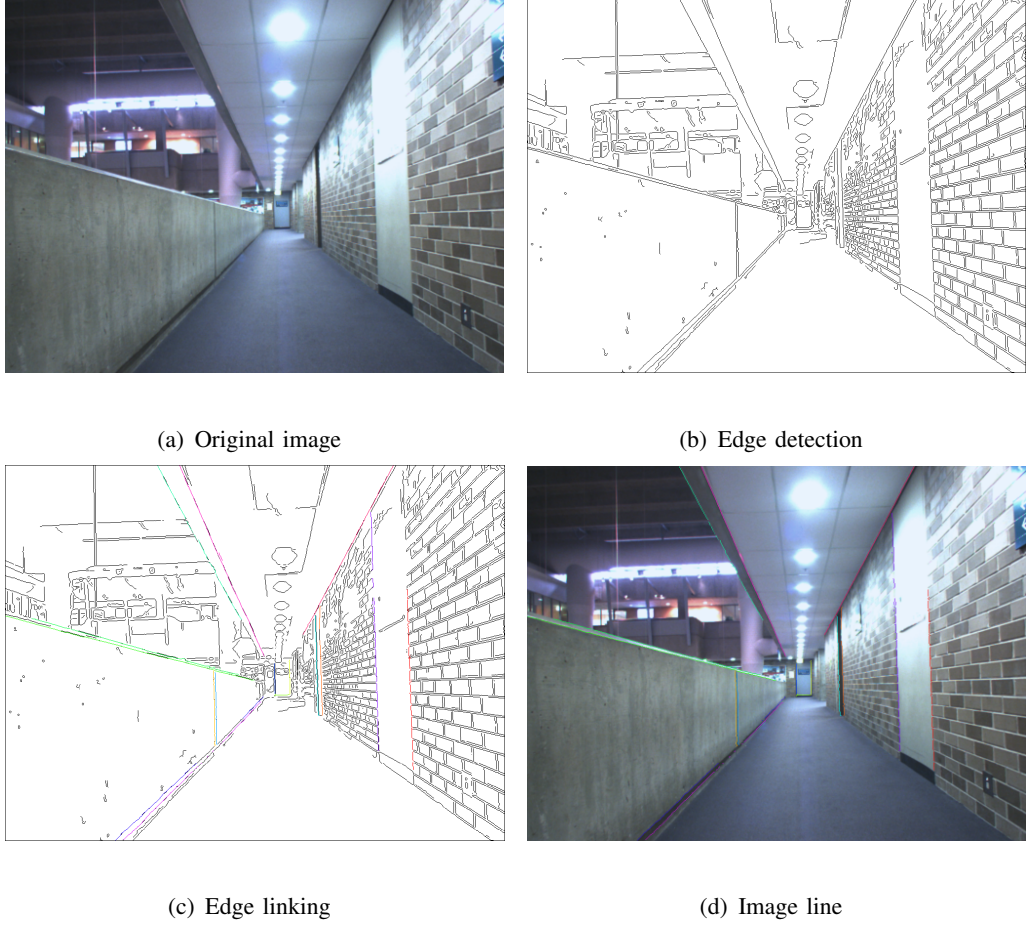


Fig. 5. Image line detection results for FEIT UTS Corridor Dataset

to the image line defined by the endpoints. The image line linking result is shown in Fig. 5(c) and Fig. 5(d).

The BA with proposed line feature parametrization is implemented using 14 images taken from one end to the other of the corridor involving 31 line features. For comparison, the BA using point features is also performed based on the SIFT feature extraction and matching, multi-level RANSAC and parallax angle feature parametrization as described in [21]. There are 6150 point features and the mean square error of the reprojections converged to 0.5967. So we believe the result of BA using point features is reasonable and use it as the benchmark. The BA result using proposed line feature parametrization and the BA result by using the point features are

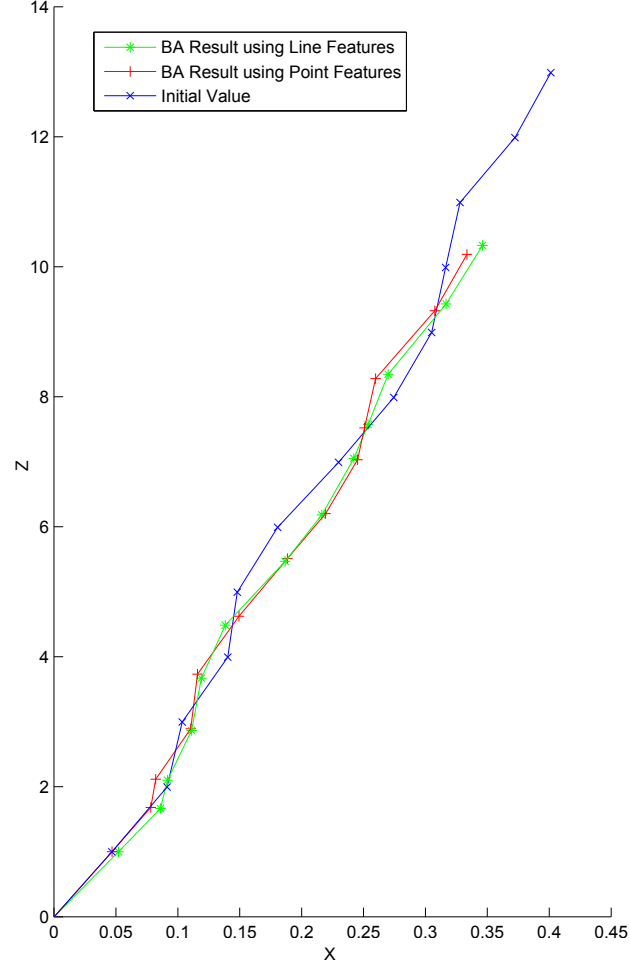


Fig. 6. Comparison of BA using only line features and BA using only point features for FEIT UTS Corridor Dataset

shown in Fig. 6 as green and red lines, respectively.

2) *ETSI Málaga corridor 2.2 Dataset*: The ETSI Málaga corridor 2.2 Dataset is a publicly available dataset collected in the corridor of ETSI Telecomunicacion, University of Málaga. The odometry, SICK LMS, HOKUYO LMS and 320x240 @ 20Hz Stereo camera data are logged from a Sancho robot [28].

Two hundred and forty images captured by the left camera are chosen to be used in this experiment. The vertical lines between doors and walls, and the corridor direction lines at the intersection of floor and wall (or ceiling and wall) are used for the proposed algorithms. For the

line feature extraction and matching, we used an approach similar to [32] together with some prior knowledge about the environment. For the vertical lines, only the lines between doors and walls are extracted and only the first 4 lines are extracted from each side of the walls. First, the start point of a line is detected by the high horizontal gradient of the intensity image because the walls are white and the doors are nearly black. And then, the edge points of the line are searched at the start point and linked together from the binary image after Canny edge detection. Each line also has a polarity defined by the sign of the gradient. Because the polarity is changed alternately, this information can be used to reject the wrong line and match the lines. At last, a line RANSAC [33] is used to remove the outlier edge points from the image line. For the 4 corridor direction lines at the intersection of floor/ceiling and wall, the normalized image line coordinates are manually computed for the very first image. Then the edge points are linked by searching the edge points whose distance to the image line is less than 6 pixels. The line RANSAC is used after linking the edge points to fit the line and remove the outliers. Because of the high framerate (20Hz), we suppose the two consecutive images do not change much and simply use the image line coordinates in the previous image to define a hypothetical line in the next image and perform a local extraction. Image line extraction results are shown in Fig. 7.

There are 240 poses, 28 line features and 2880 image line observations involved in the global BA. The proposed BA with GN takes 63 iterations, and the final MSE is 25.9175. The computational cost of the global BA is 332 seconds. And then the 240 images are divided into 3 groups to build 3 local maps. Each local map contains about 80 to 81 poses and 16 to 19 line features, and is also built by the proposed BA. Then the proposed map joining algorithm is used to join the local maps together to get the global map. Cost of computing each local map was between 12 to 38 seconds. Deleting features, poses and computing information matrix of each local map took about 0.3 to 0.5 seconds. The map joining took 22 seconds to build the global map including 75 poses or translations and 28 line features. The total time of local map building plus map joining is 89 seconds. The global BA result and map joining result are shown in Fig. 8 with green and blue lines, respectively. For comparison, the pose graph SLAM

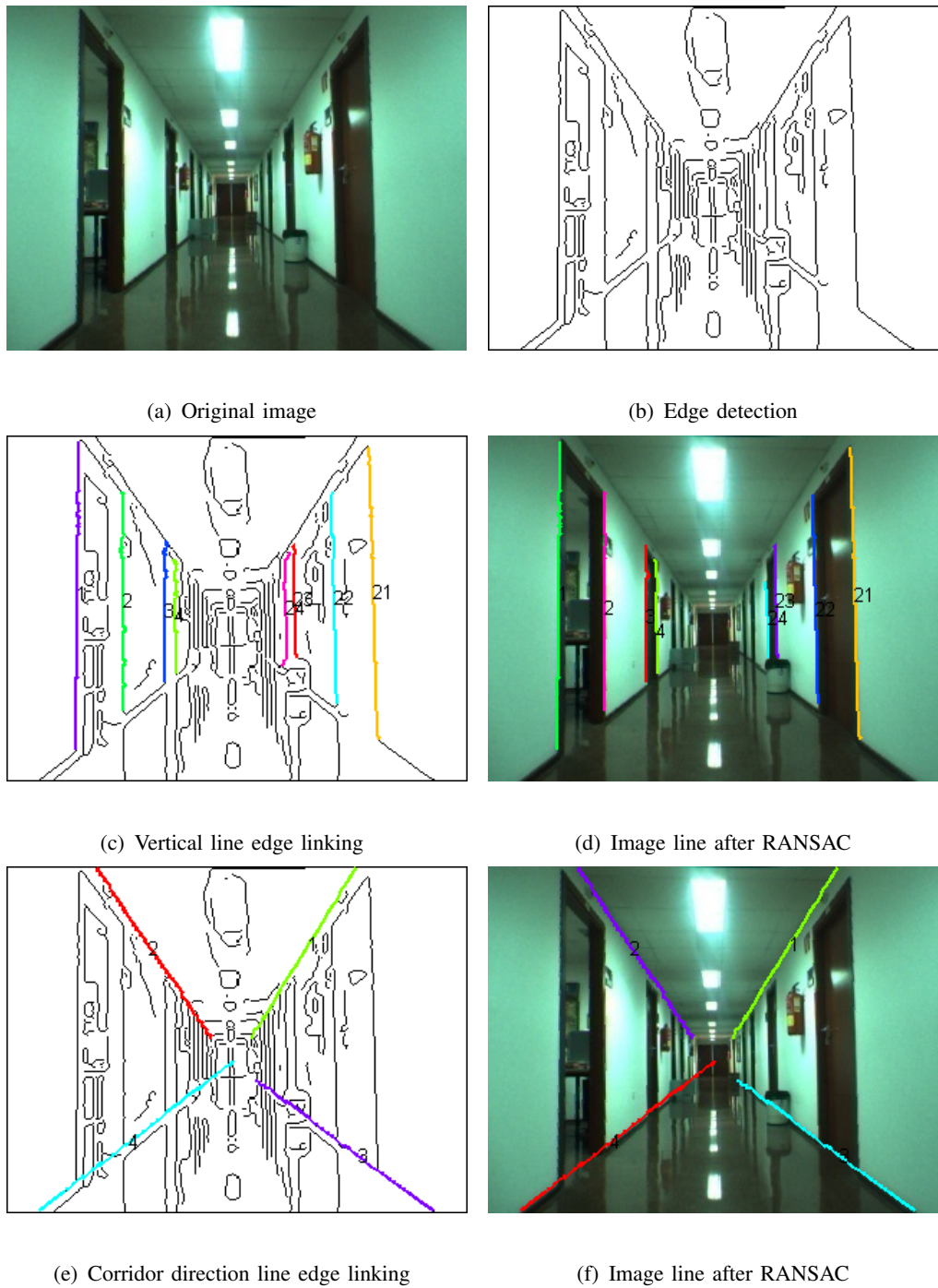


Fig. 7. Image line detection results for ETSI Málaga corridor 2.2 Dataset

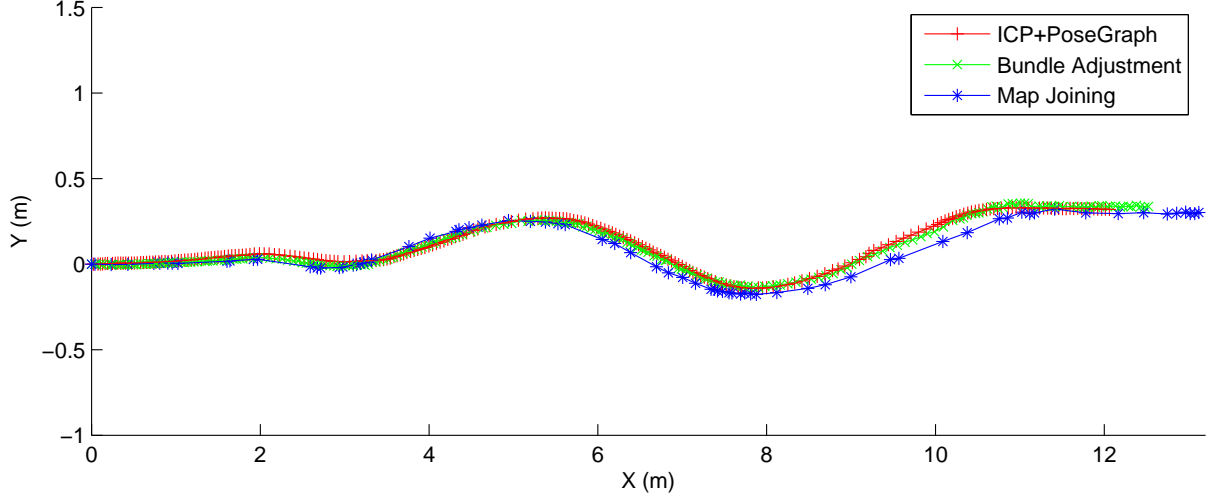
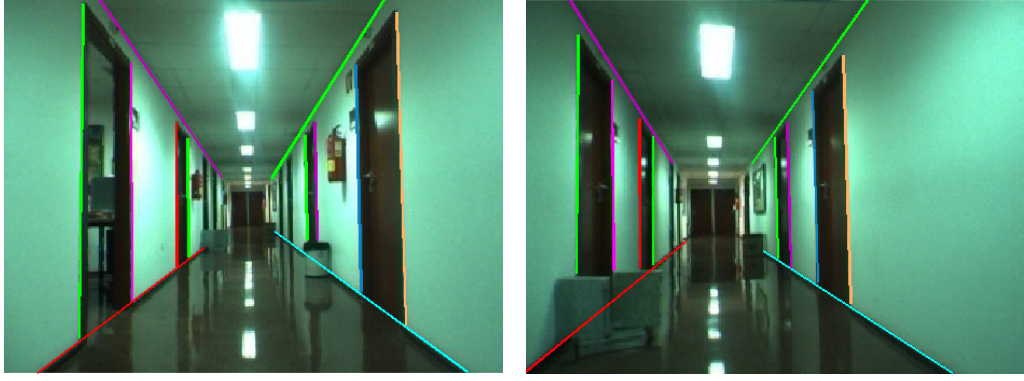


Fig. 8. BA, map joining and pose graph SLAM results of ETSI Málaga corridor 2.2 Dataset

result based on ICP using the backward 2D laser scans is also shown in Fig. 8 with red line, which is arguably the best result one can achieve in this kind of environment. BA_OR algorithm is also implemented. When GN is used, both BA_OR_1 and BA_OR_2 directly diverged. And when LM is used, both BA_OR_1 and BA_OR_2 converge to the same MSE as 25.9175. While the iteration numbers are 488 and 481, respectively.

The 3D line features are reprojected to the image lines in different images using the estimated poses and line features obtained through BA and computed by the observation function proposed in this paper. The image line reprojection results for two randomly selected images (image 1 and image 128, endpoints are manually given) are shown in Fig. 9.

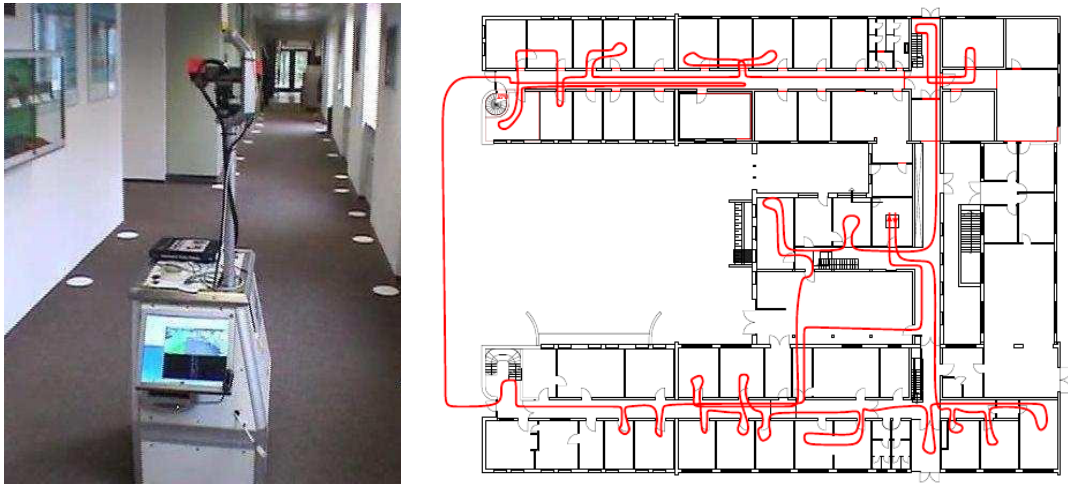
3) *DLR Dataset*: Another large-scale publicly available dataset with multiple loops is also used to test the BA and map joining algorithms proposed in this paper. The dataset was recorded at a corridor environment in the DLR (Deutsches Zentrum für Luft und Raumfahrt), Institute of Robotics and Mechatronics building by a mobile robot (Fig. 10(a)). So it is also a line structured environment and ideal for the proposed SLAM algorithms. As described in [29], the building covers a region of $60m \times 45m$ and the robot path consists of three large loops within the building



(a) Image 1

(b) Image 128

Fig. 9. Image line reprojection using BA result for ETSI Málaga corridor 2.2 Dataset



(a) Robot

(b) Architectural map and robot trajectory

Fig. 10. The robot, architectural map and the robot path for DLR dataset

(plus a small outside path) with a total length of 505 meters. On the way the robot visits 29 rooms. The architectural map of the building and the robot trajectory are shown in Fig. 10(b).

There are two kinds of features in the environment, one is artificial circular disks and the other is vertical lines in the office environment which can be door frames, images at the wall, lockers and so on. Then these features are captured by one of the Sony EVI-371DG camera. The camera calibration parameters can also be found in the dataset [29]. In this experiment, the

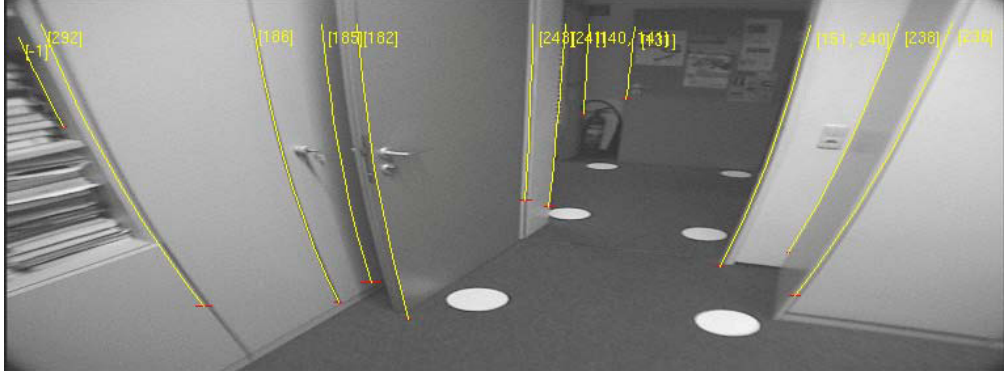


Fig. 11. Line features data association in DLR dataset

vertical line features are used in the proposed BA and map joining algorithms. Feature extraction and data association results are given in the dataset (Fig. 11). Because there is no line features along the outside path of the robot trajectory, the odometry is needed in BA to deal with the lack of information.

There are 3298 poses, 1206 3D line features, 15653 image line observations and 3297 odometry observations in total. The proposed BA algorithm takes 853 seconds to get the global BA result. The final objective function is 3024.6731 (Here we use objective function instead of MSE because the odometry is involved). The global BA result is shown in Fig. 12 as green dots. Then the whole dataset is divided into 4 groups to build 4 local maps. Each local map contains about 825 to 826 poses and 295 to 412 line features. The local maps are first built by the BA proposed in this paper, and then the proposed map joining algorithm is used to join the local maps together to get the global map. Cost of computing each local map was between 18 to 31 seconds. Deleting features, poses and computing information matrix of each local map took about 11 to 20 seconds. The map joining took 128 seconds to build the global map including 626 poses or translations and 234 line features. The total time of local map building plus map joining is 286 seconds. The map joining result is shown in Fig. 12 as blue dots. As the benchmark for comparison, the range and bearing result using artificial circular disks as landmarks is also shown in Fig. 12 as

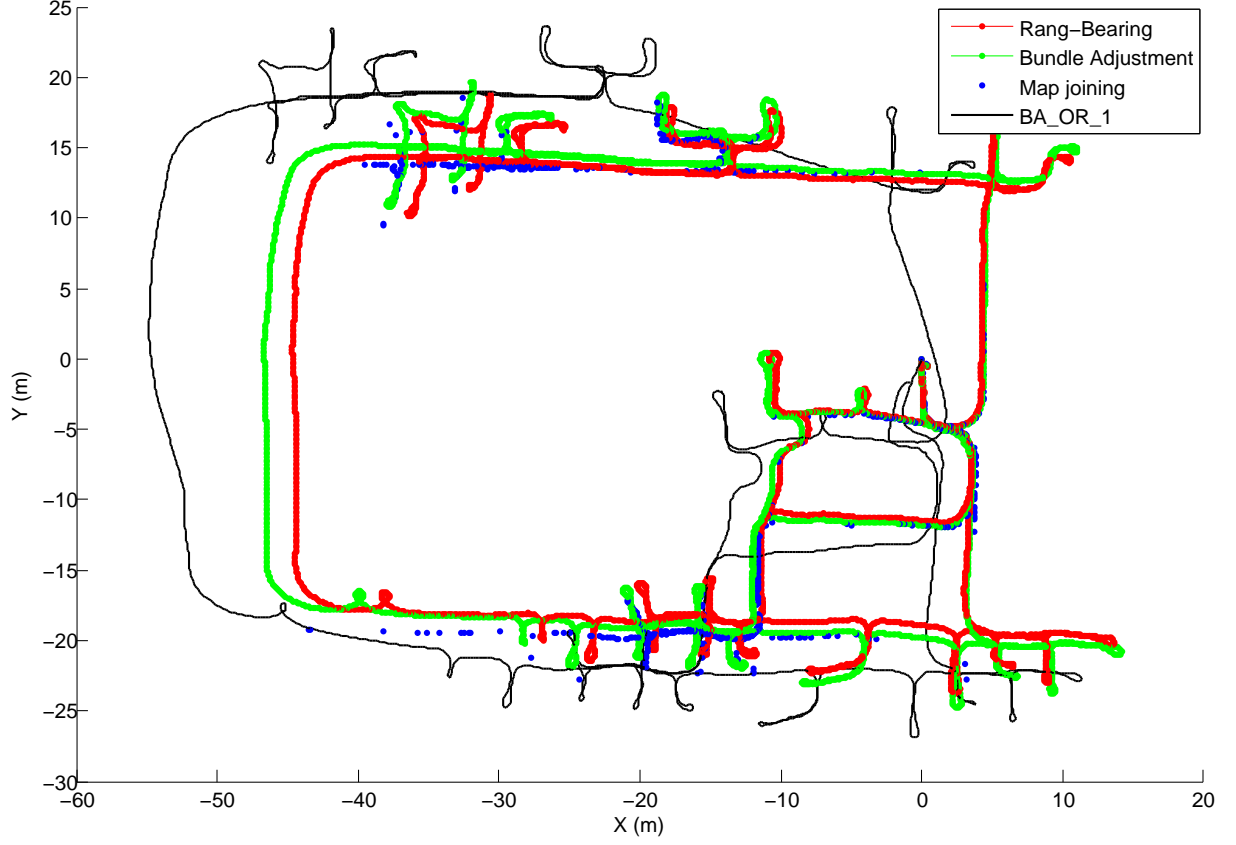


Fig. 12. BA and map joining results of DLR dataset

red dots. As in simulation, both BA_OR_1 and BA_OR_2 cannot converge using GN. And when LM is used, the objective functions of BA_OR_1 and BA_OR_2 converge to 34224.6981 and 34756.7019 respectively, which are obvious local minima. The LM result of BA_OR_1 is also shown in Fig. 12 as black line.

Table VI and Table VII summarize the computational cost and the convergence of the different algorithms using the ETSI Málaga and DLR datasets.

VII. CONCLUSION AND FUTURE WORKS

This paper presents a new approach to represent line features in monocular SLAM. The line feature considered in this paper is the straight line with unknown endpoints. Each line feature

TABLE VI

COMPUTATIONAL COST OF GLOBAL BA AND MAP JOINING OF REAL EXPERIMENTS (IN SECONDS)

Dataset	Pose	3D Line	Image Line	Global BA		Map Joining		
					Local BA	Schur	Map Joining	Total
ETSI Málaga	240	28	2880	332	12–38	0.3–0.5	22	89
DLR	3298	1206	15653	853	18–31	11–20	128	286

*Implemented in Matlab, run on an Intel E8400@3.0GHz CPU, 4.0G RAM, code is not optimized.

TABLE VII

CONVERGENCE AND MSE/OBJECTIVE FUNCTION OF REAL EXPERIMENTS

Dataset	BA	BA_OR_1		BA_OR_2	
	GN	GN	LM	GN	LM
ETSI Málaga	25.9175	N	25.9175	N	25.9175
DLR	3024.6731	N	34224.6981	N	34756.7019

observed once is presented by its back-projected plane, while each line feature observed at least twice is presented by two of its back-projected planes. Each back-projected plane is presented by its normal with the associated camera centre as the anchor and each normal is parametrized by a pair of azimuth and elevation angles.

The bundle adjustment algorithm using the proposed line feature parametrization is developed for monocular SLAM with only line features. Because the anchored camera centres are already present in the state vector of BA, this leads to a minimal line feature parametrization, that is, 2 parameters for each line observed only once, and 4 parameters for each 3D line feature. An important property of the new feature parametrization is that a good initial value can always be guaranteed as these parameters can be directly computed from the information obtained from

the measurement.

A map joining algorithm based on the proposed line feature parametrization is also presented. Together with local maps built by BA, the algorithms are able to simultaneously optimize the camera poses, feature positions and the relative scales. Simulation and experimental results demonstrated the effectiveness and consistency of the proposed BA and map joining algorithms using the new line feature parametrization.

Unlike the point features, robust line feature extraction and matching from image data still remains a challenge. In the current experimental results shown in this paper, the line feature matching involves some manual operations and prior knowledge of the line features. In the next step, we are planning to improve the line feature extraction and matching algorithm such that the proposed BA algorithm can be applied more robustly to general indoor environments. Moreover, the relationship between the proposed line feature parametrization and the SP-Map representation [34] needs further investigation. Monocular SLAM using both point features and line features is straightforward by combining the point feature parametrization in [21] and the line feature parametrization proposed in this paper.

REFERENCES

- [1] A. J. Davison, "Real-time Simultaneous Localisation and Mapping with a Single Camera," *Proceedings of the International Conference on Computer Vision (ICCV)*, vol. 2, pp. 1403-1410 (2003).
- [2] G. Klein and D. Murray, "Improving the Agility of Keyframe-based SLAM," *Proceedings of the 10th European Conference on Computer Vision (ECCV)*, Marseille, pp. 802-815 (2008).
- [3] J. Sola, T.V. Calleja, J. Civera and J.M.M. Montiel, "Impact of landmark parametrization on monocular EKF-SLAM with points and lines," *International Journal of Computer Vision*, **97**(3), 339-368 (2012).
- [4] D. Simon and T.L. Chia, "Kalman Filtering with State Equality Constraints," *IEEE Transactions on Aerospace and Electronic Systems*, **38**(1), 128-136 (2002).
- [5] S. J. Julier and J. J. LaViola, "On Kalman Filtering with Nonlinear Equality Constraints," *IEEE Transactions on Signal Processing*, **55**(6), 2774-2784 (2007).

- [6] A. Bartoli and P. Sturm, "Structure-from-motion using Lines: Representation, Triangulation and Bundle Adjustment," *Computer Vision and Image Understanding*, **100**(3), 416-441 (2005).
- [7] H. Strasdat, J. M. M. Montiel and A. J. Davison, "Real-time Monocular SLAM: Why Filter?" *Proceedings of the IEEE International Conference on Robotics and Automation (ICRA)*, Anchorage, USA, pp. 2657-2664 (May 2010).
- [8] K. Konolige and M. Agrawal, "FrameSLAM: From Bundle Adjustment to Real-Time Visual Mapping," *IEEE Transactions on Robotics*, **24**(5), 1066-1077 (Oct. 2008).
- [9] S. Huang, Z. Wang and G. Dissanayake, "Sparse Local Submap Joining Filter for Building Large-Scale Maps," *IEEE Transactions on Robotics*, **24**(5), 1121-1130 (Oct. 2008).
- [10] E. Eade and T. Drummond, "Edge Landmarks in Monocular SLAM," *Image and Vision Computing*, **27**, 588-596 (2009).
- [11] G. Klein and D. Murray, "Full-3D Edge Tracking with A Particle Filter," *Proceedings of the British Machine Vision Conference (BMVC)*, Edinburgh, vol. 3, pp. 1119-1128 (2006).
- [12] P. Smith, I. Reid and A. J. Davison, "Real-time Monocular SLAM with Straight Lines," *Proceedings of the British Machine Vision Conference (BMVC)*, Edinburgh, vol. 1, pp. 17-26 (2006).
- [13] A. P. Gee and W. Mayol-Cuevas, "Real-Time Model-Based SLAM using Line Segments," *2nd International Symposium on Visual Computing*, vol. 4292, pp. 354-363 (Nov. 2006).
- [14] C. J. Taylor and D. J. Kriegman, "Structure and Motion from Line Segments in Multiple Images," *IEEE Transactions on Pattern Analysis and Machine Intelligence*, **17**(11), 1021-1032 (1995).
- [15] T. Lemaire and S. Lacroix, "Monocular-vision Based SLAM using Line Segments," *Proceedings of the IEEE International Conference on Robotics and Automation (ICRA)*, Rome, Italy, pp. 2791-2796 (2007).
- [16] J. Sola, T. Vidal-Calleja and M. Devy, "Undelayed Initialization of Line Segments in Monocular SLAM," *Proceedings of the IEEE/RSJ International Conference on Intelligent Robots and Systems (IROS)*, Saint Louis, USA, pp. 1553-1558 (Oct. 2009).
- [17] T. Vidal-Calleja, C. Berger, J. Sola and S. Lacroix. "Large Scale Multiple Robot Visual Mapping with Heterogeneous Landmarks in Semi-Structured Terrain," *Robotics and Autonomous Systems*, **59**, 654-674 (2011).
- [18] R. Hartley and A. Zisserman, "Multiple View Geometry in Computer Vision," 2nd Ed., (Cambridge University Press, 2003).
- [19] G. Hu, S. Huang and G. Dissanayake, "3D I-SLSJF: A Consistent Sparse Local Submap Joining Algorithm for Building Large-Scale 3D Maps," *Proceedings of the 48th IEEE Conference on Decision and Control*, Shanghai, China, pp. 6040-6045 (2009).
- [20] L. Zhao, S. Huang, L. Yan, J. Wang, G. Hu and G. Dissanayake, "Large-Scale Monocular SLAM by Local Bundle

- Adjustment and Map Joining,” *Proceedings of the 11th International Conference on Control, Automation, Robotics and Vision (ICARCV)*, Singapore, pp. 431-436 (Dec. 2010).
- [21] L. Zhao, S. Huang, L. Yan and G. Dissanayake, “Parallax Angle Parametrization for Monocular SLAM,” *Proceedings of the IEEE International Conference on Robotics and Automation (ICRA)*, Shanghai, China, pp. 3117-3124 (May 2011).
 - [22] H. Strasdat, J. M. M. Montiel and A. J. Davison, “Scale Drift-Aware Large Scale Monocular SLAM,” *Proceedings of the Robotics: Science and Systems Conference (RSS)* (2010).
 - [23] C. Estrada, J. Neira and J.D. Tardos. “Hierarchical SLAM: Real-time Accurate Mapping of Large Environments,” *IEEE Transactions on Robotics*, **21**(4), pp. 588-596 (2005).
 - [24] E. Mouragnon, M. Lhuillier, M. Dhome, F. Dekeyser and P. Sayd, “Generic and Real Time Structure from Motion using Local Bundle Adjustment,” *Image and Vision Computing*, **27**(8), 1178-1193 (2009).
 - [25] L. M. Paz and J. Neira, “Optimal Local Map Size for EKF-based SLAM,” *Proceedings of the IEEE/RSJ International Conference on Intelligent Robots and Systems (IROS)*, Beijing, China, pp. 9-15 (Oct. 2006).
 - [26] S. Huang and G. Dissanayake, “Convergence and Consistency Analysis for Extended Kalman Filter Based SLAM,” *IEEE Transactions on Robotics*, **23**(5), 1036-1049 (2007).
 - [27] S. Huang, Z. Wang, G. Dissanayake and U. Frese, “Iterated D-SLAM Map Joining: Evaluating Its Performance in Terms of Consistency, Accuracy and Efficiency,” *Autonomous Robots*, **27**, 409-429 (2009).
 - [28] J. L. Blanco, “Mobile Robot Programming Toolkit (MRPT),” [Online]. Available: <http://www.mrpt.org/node/239/>.
 - [29] J. Kurlbaum and U. Frese, “A Benchmark Data Set for Data Association,” [Online]. Available: <http://www.sfbtr8.uni-bremen.de/reports.htm>. Data available: <http://radish.sourceforge.net/>
 - [30] A. Kassir and T. Peynot, “Reliable Automatic Camera-Laser Calibration,” *Proceedings of Australasian Conference on Robotics and Automation (ACRA)*, Brisbane, Australia (Dec. 2010).
 - [31] J. Canny. “A Computational Approach to Edge Detection”, *IEEE Transactions on Pattern Analysis and Machine Intelligence*, **8**(6), 679-98 (Nov. 1986).
 - [32] P. Neubert, P. Protzel, T. Vidal-Calleja and S. Lacroix, “A Fast Visual Line Segment Tracker,” *Proceedings of IEEE International Conference on Emerging Technologies and Factory Automation*, Hamburg, Germany, pp. 353-360 (Sep. 2008).
 - [33] P. D. Kovesi, “MATLAB and Octave Functions for Computer Vision and Image Processing,” Centre for Exploration Targeting, School of Earth and Environment, The University of Western Australia, [Online]. Available: <http://www.csse.uwa.edu.au/pk/research/matlabfns/>.
 - [34] J. A. Castellanos, J. M. M. Montiel, J. Neira and J. Tardos, “The SPmap: A Probabilistic Framework for Simultaneous

Localization and Map Building,” *IEEE Transactions on Robotics and Automation*, **15**, 948-953 (1999).